Robotica (2015) volume 33, pp. 413–435. © Cambridge University Press 2014
doi:10.1017/S0263574714000253

# Optimization-based dynamic 3D human running prediction: effects of foot location and orientation

Hyun-Joon Chung†, Yujiang Xiang‡*, Jasbir S. Arora† and Karim Abdel-Malek†

† *Center for Computer-Aided Design (CCAD), The University of Iowa, Iowa City, IA 52242, USA*
‡ *Department of Mechanical Engineering, University of Alaska Fairbanks, Fairbanks, AK 99775, USA*

(Accepted February 2, 2014. First published online: March 4, 2014)

**SUMMARY**
This paper presents optimization-based dynamic three-dimensional (3D) human running prediction. A predictive dynamics method is used to formulate the running problem, and normal running is formulated as a symmetric and cyclic motion. In addition, a slow jog along curved paths has been formulated. It is a non-symmetric running motion, so a stride formulation has been used. The dynamic effort and impulse are used as the performance measure, and the upper body yawing moment is also included in the performance measure. The joint angle profiles and joint torque profiles are calculated for the full-body human model, and the ground reaction force is determined. The effects of foot location and orientation on the running motion prediction are simulated and studied. Simulation results from this methodology show good correlation with experimental data obtained from human subjects.

KEYWORDS: Running; Slow jog; Impulse; Arm swing; Optimization.

## 1. Introduction

In recent years, virtual human modeling has received considerable interest in many fields to simulate real-world tasks. Various motions of the model are required, especially the running motion, which has been studied in both the robotics and biomechanics fields.[1–10] Nagasaki *et al.*[6] generated the running pattern by using the conservation of angular momentum and the control theory. Park and Kwon[9] developed a biped robot's running motion by using impedance control. Fujimoto[1] presented a method to generate the trajectory of a biped robot that has five links. The energy consumption was minimized during running simulation. In review papers, Õunpuu[8] and Novacheck[7] reviewed and summarized the joint angles and joint torques during human running.

In addition, there have been a growing number of studies in the use of running for training and rehabilitation purposes. For this purpose, the running characteristics have been studied using experimental methods.[11,12] Milliron and Cavanagh[11] synthesized the data available in the literature for the lower extremities for planar motion and showed how such data can be extended to obtain insights for the mechanics of running. Simpson and Bates[12] experimented with the effect of running speed on joint moments in the support phase using a motion capture method. They calculated the joint moments of the lower extremities using the data from motion capture and the ground reaction force (GRF) from a force plate. Then, the effects of running speed on joint moments were investigated.

Recently, there has been more progress in optimization-based methods to simulate complex human motion using large-scale mechanical models.[13–19] The predictive dynamics method[20,21] is an efficient optimization-based method to simulate human motions. The major advantage of the method lies in its computational efficiency, because inverse dynamics are used to evaluate joint torque in an optimization iteration process instead of using a forward numerical integration approach. In addition, this method

* Corresponding author. E-mail: yujxiang@gmail.com

https://doi.org/10.1017/S0263574714000253 Published online by Cambridge University Press

does not need full motion or force profile history for all joints, making it more suitable for use with human motion simulation. The predictive dynamics method has been used successfully to simulate walking,[16,17] box lifting,[18,19] and throwing motions,[22,38] and some biomechanical insights have been obtained from these simulations.

Kim *et al.*[4] studied yawing moment cancellation and zero moment point (ZMP) compensation for the humanoid robot to avoid the possible slipping on the ground caused by the yawing moment. So, they postulated that the upper-body motion of the robot should compensate for the yawing moment. Collins *et al.*[23] studied arm swing motion in human walking. Their hypothesis was that the reduction of ground reaction moment may explain the physiological benefit of arm swinging. From the experimental measurements of humans, they observed the arm swinging motion most affected by the vertical ground reaction moment.

The goal of this study is to formulate, simulate, and analyze the running of a full human-body model using the predictive dynamics method; in particular, the effects of foot location and orientation on running motion are studied. The contents of the paper are organized as follows. Section 2 introduces kinematics and dynamics of the human body based on the Denavit–Hartenberg (DH)[24] method. Section 3 presents dynamics equilibrium based on ZMP and impulse. Section 4 presents a running model. Section 5 shows a detailed optimization formulation for the running problem. Section 6 presents the clamped B-spline discretization and Section 7 demonstrates the various running simulation results with different foot location and orientation. Finally, conclusions are given in Section 8.

## 2. Kinematics and Dynamics of Human Model

### *2.1. 3D skeletal model: Denavit–Hartenberg method*

A digital human is modeled as a mechanical system that includes link lengths, mass moments of inertia, joint torques, and external forces. The entire model has 55 degrees of freedom (DOFs)—6 DOFs for global translation and rotation, and 49 DOFs for the body. The DH method is applied for the kinematics analysis. This method represents each link coordinate system in terms of the previous link coordinate system. Any local coordinate system can be expressed in the global reference frame by the DH method.

Any point of interest in the $i$th frame ${}^{i}\mathbf{x}$ can be transferred to the global reference frame ${}^{0}\mathbf{r}$:

$$ {}^{0}\mathbf{r} = {}^{0}\mathbf{T}_i \, {}^{i}\mathbf{r}, \tag{1} $$

where ${}^{i}\mathbf{r}$ is a $4 \times 1$ vector in terms of the $i$th reference frame and ${}^{0}\mathbf{T}_i$ is a $4 \times 4$ homogeneous transformation matrix from the $i$th reference frame to the global reference frame. The format of the vector ${}^{i}\mathbf{r}$ is

$$ {}^{i}\mathbf{r} = \begin{bmatrix} r_x & r_y & r_z & 1 \end{bmatrix}^T, \tag{2} $$

where $r_x$, $r_y$, and $r_z$ represent any point of interest in the $i$th frame in terms of the Cartesian coordinates.

Here the transformation of a vector to the global reference frame is simply the multiplication of transformation matrices, which is given as

$$ {}^{0}\mathbf{T}_i = {}^{0}\mathbf{T}_1 \, {}^{1}\mathbf{T}_2 \ldots {}^{i-1}\mathbf{T}_i = \prod_{n=1}^{i} {}^{n-1}\mathbf{T}_n. \tag{3} $$

According to the DH method, the four DH parameters in Fig. 1 are defined as $\theta_i$, $d_i$, $a_i$, and $\alpha_i$, which relate coordinate frames $i$ and $i-1$. The DH transformation matrix from the $i-1$th frame to the $i$th frame is then given as

$$ {}^{i-1}\mathbf{T}_i = \begin{bmatrix} \cos\theta_i & -\cos\alpha_i \sin\theta_i & \sin\alpha_i \sin\theta_i & a_i \cos\theta_i \\ \sin\theta_i & \cos\alpha_i \cos\theta_i & -\sin\alpha_i \cos\theta_i & a_i \sin\theta_i \\ 0 & \sin\alpha_i & \cos\alpha_i & d_i \\ 0 & 0 & 0 & 1 \end{bmatrix}. \tag{4} $$

https://doi.org/10.1017/S0263574714000253 Published online by Cambridge University Press

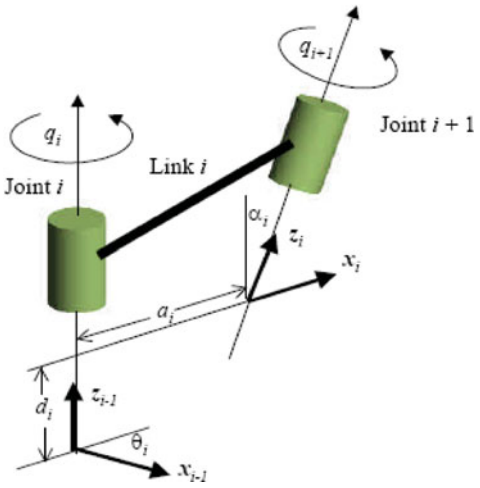



Fig. 1. DH parameters.

In the case of a rotational joint, the joint parameters $d_i$, $a_i$, and $\alpha_i$ are constant (which means they are fixed). Only $\theta_i$ is treated as a rotational DOF, $q_i$. In a mechanical model, $q_i$ is the vector of generalized coordinates, and each transformation matrix has one DOF.

The global DOFs are composed of three translational (prismatic) joints and three rotational (revolute) joints that move the mechanical model around with respect to an inertial reference frame. There are 49 DOFs for the local body frame according to the DH method. A full-body digital human model is described in Fig. 2.

### 2.2. *Kinematic analysis of the human body*

The kinematics analysis in the recursive form leads to a simpler form for the transformation matrix $\mathbf{A}_i$. The time derivatives of the transformation matrix $\mathbf{A}_i$ can be obtained in the recursive form as well:

$$\mathbf{A}_i = \mathbf{A}_{i-1}{}^{i-1}\mathbf{T}_i, \tag{5}$$

$$\mathbf{B}_i = \dot{\mathbf{A}}_i = \mathbf{B}_{i-1}{}^{i-1}\mathbf{T}_i + \mathbf{A}_{i-1}\frac{\partial {}^{i-1}\mathbf{T}_i}{\partial q_i}\dot{q}_i, \tag{6}$$

$$\mathbf{C}_i = \dot{\mathbf{B}}_i = \mathbf{C}_{i-1}{}^{i-1}\mathbf{T}_i + 2\mathbf{B}_{i-1}\frac{\partial {}^{i-1}\mathbf{T}_i}{\partial q_i}\dot{q}_i + \mathbf{A}_{i-1}\frac{\partial^2 {}^{i-1}\mathbf{T}_i}{\partial q_i^2}\dot{q}_i^2 + \mathbf{A}_{i-1}\frac{\partial {}^{i-1}\mathbf{T}_i}{\partial q_i}\ddot{q}_i, \tag{7}$$

where $q_i$ is the joint angle and ${}^{i-1}\mathbf{T}_i$ is the link transformation matrix.

### 2.3. *Dynamics: recursive Lagrangian formulation*

Based on forward recursive kinematics, the backward recursion for the dynamic analysis is accomplished by defining a $4 \times 4$ transformation matrix $\mathbf{D}_i$ and $4 \times 1$ transformation vectors $\mathbf{E}_i$, $\mathbf{F}_i$, and $\mathbf{G}_i$ as follows: given the mass and inertia properties of each link, the external force $\mathbf{f}_k^{\mathrm{T}} = [\,{}^k f_x \; {}^k f_y \; {}^k f_z \; 0\,]$ and the moment $\mathbf{h}_k^{\mathrm{T}} = [\,{}^k h_x \; {}^k h_y \; {}^k h_z \; 0\,]$ for link $k$, defined in the global coordinate system, the joint actuation torques $\tau_i$ for $i = n$ to 1, are computed as[25–27]

$$\tau_i = \mathbf{tr}\left[\frac{\partial \mathbf{A}_i}{\partial q_i}\mathbf{D}_i\right] - \mathbf{g}^{\mathrm{T}}\frac{\partial \mathbf{A}_i}{\partial q_i}\mathbf{E}_i - \mathbf{f}_k^{\mathrm{T}}\frac{\partial \mathbf{A}_i}{\partial q_i}\mathbf{F}_i - \mathbf{G}_i^{\mathrm{T}}\mathbf{A}_{i-1}\mathbf{z}_0, \tag{8}$$

$$\mathbf{D}_i = \mathbf{J}_i\mathbf{C}_i^{\mathrm{T}} + \mathbf{T}_{i+1}\mathbf{D}_{i+1}, \tag{9}$$

$$\mathbf{E}_i = m_i{}^i\mathbf{r}_i + \mathbf{T}_{i+1}\mathbf{E}_{i+1}, \tag{10}$$

$$\mathbf{F}_i = {}^k\mathbf{r}_f\delta_{ik} + \mathbf{T}_{i+1}\mathbf{F}_{i+1}, \tag{11}$$

$$\mathbf{G}_i = \mathbf{h}_k\delta_{ik} + \mathbf{G}_{i+1}, \tag{12}$$

https://doi.org/10.1017/S0263574714000253 Published online by Cambridge University Press

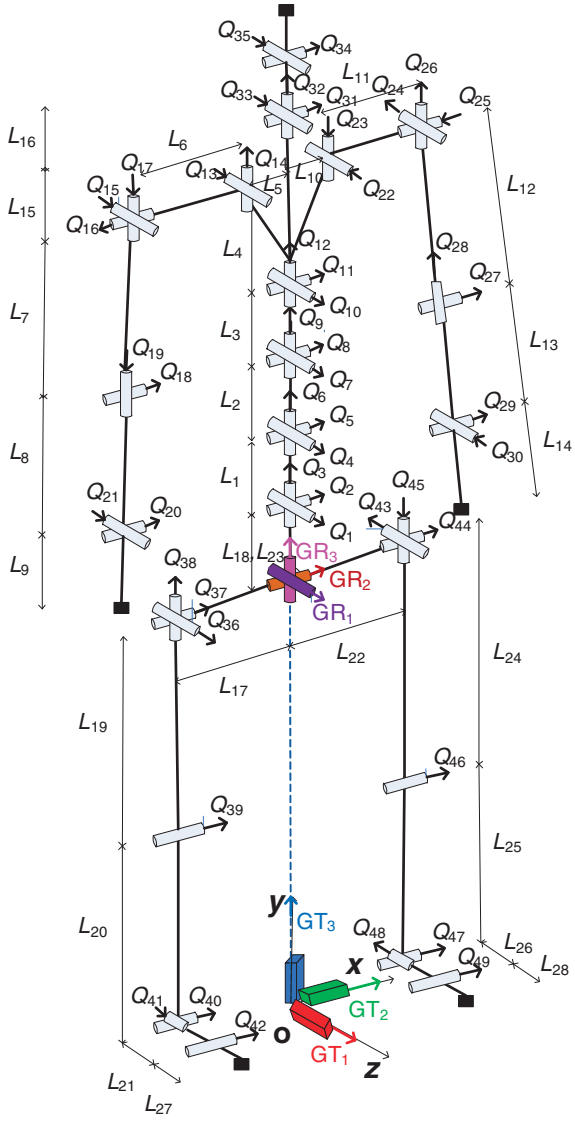



Fig. 2. Local coordinate system of human model based on DH method.

where $\mathbf{D}_{n+1} = 0$ and $\mathbf{E}_{n+1} = \mathbf{F}_{n+1} = \mathbf{G}_{n+1} = 0$; $\mathbf{J}_i$ is the inertia matrix for link $i$; $m_i$ is the mass of link $i$; $\mathbf{g}$ is the gravity vector; ${}^{i}\mathbf{r}_i$ is the location of center of mass of link $i$ in the local frame $i$; ${}^{k}\mathbf{r}_f$ is the position of the external force in the local frame $k$; $\mathbf{z}_0 = \begin{bmatrix} 0 & 0 & 1 & 0 \end{bmatrix}^{\mathbf{T}}$ for a revolute joint and $\mathbf{z}_0 = \begin{bmatrix} 0 & 0 & 0 & 0 \end{bmatrix}^{\mathbf{T}}$ for a prismatic joint; and, finally, $\delta_{ik}$ is Kronecker delta.

The first term in the torque expression (equation of motion, EOM) is the inertia and Coriolis torque, the second term is the torque due to gravity load, the third term is the torque due to external force, and the fourth term represents the torque due to the external moment.

The derivatives, $\frac{\partial \tau_i}{\partial q_k}$, $\frac{\partial \tau_i}{\partial \dot{q}_k}$, $\frac{\partial \tau_i}{\partial \ddot{q}_k}$ ($i = 1$ to $n$; $k = 1$ to $n$), can be evaluated for the articulated spatial human mechanical system in a recursive way using the foregoing recursive Lagrangian dynamics formulation as follows:[26,27]

$$\frac{\partial \tau_i}{\partial q_k} = \begin{cases} \mathbf{tr}\left(\frac{\partial^2 \mathbf{A}_i}{\partial q_i \partial q_k}\mathbf{D}_i + \frac{\partial \mathbf{A}_i}{\partial q_i}\frac{\partial \mathbf{D}_i}{\partial q_k}\right) - \mathbf{g}^{\mathbf{T}}\frac{\partial^2 \mathbf{A}_i}{\partial q_i \partial q_k}\mathbf{E}_i - \mathbf{f}^{\mathbf{T}}\frac{\partial^2 \mathbf{A}_i}{\partial q_i \partial q_k}\mathbf{F}_i - \mathbf{G}_i^{\mathbf{T}}\frac{\partial \mathbf{A}_{i-1}}{\partial q_k}\mathbf{z}_0 & (k \le i) \\ \mathbf{tr}\left(\frac{\partial \mathbf{A}_i}{\partial q_i}\frac{\partial \mathbf{D}_i}{\partial q_k}\right) - \mathbf{g}^{\mathbf{T}}\frac{\partial \mathbf{A}_i}{\partial q_i}\frac{\partial \mathbf{E}_i}{\partial q_k} - \mathbf{f}^{\mathbf{T}}\frac{\partial \mathbf{A}_i}{\partial q_i}\frac{\partial \mathbf{F}_i}{\partial q_k} & (k > i) \end{cases}, \quad (13)$$

https://doi.org/10.1017/S0263574714000253 Published online by Cambridge University Press

$$\frac{\partial \tau_i}{\partial \dot{q}_k} = \mathbf{tr}\left(\frac{\partial \mathbf{A}_i}{\partial q_i}\frac{\partial \mathbf{D}_i}{\partial \dot{q}_k}\right), \tag{14}$$

$$\frac{\partial \tau_i}{\partial \ddot{q}_k} = \mathbf{tr}\left(\frac{\partial \mathbf{A}_i}{\partial q_i}\frac{\partial \mathbf{D}_i}{\partial \ddot{q}_k}\right). \tag{15}$$

## 3. Dynamic Stability: ZMP and Impact

### *3.1. ZMP and ground reaction forces*

An important consideration for the running problem is the dynamic stability of the motion. The most common constraint for achieving stability for biped gait analysis is the ZMP constraint in the support phase. If the $x$–$z$ plane is considered as the ground, as shown in Fig. 2, the normal vector $\mathbf{n}$ is $\begin{bmatrix} 0 & 1 & 0 \end{bmatrix}^T$. Then, the ZMP can be calculated as[28]

$$z_{\text{zmp}} = \frac{\sum_i^n [m_i(-\ddot{y}_i - g)z_i + m_i \ddot{z}_i y_i] + \dot{H}_{Gx}}{\sum_i^n m_i(-\ddot{y}_i - g)}, \tag{16}$$

$$x_{\text{zmp}} = \frac{\sum_i^n [m_i(-\ddot{y}_i - g)x_i + m_i \ddot{x}_i y_i] - \dot{H}_{Gz}}{\sum_i^n m_i(-\ddot{y}_i - g)}, \tag{17}$$

where $g$ is the gravitational vector value, $\dot{H}_{Gx}$ is the time derivative of angular momentum along the global $x$-axis, and $\dot{H}_{Gz}$ is the time derivative of angular momentum along the global $z$-axis.

In addition, a two-step algorithm is used to calculate the GRF to obtain the joint torques for the multibody human system. Details of the algorithm are presented by Xiang *et al.*[16] and outlined here as follows:

First, the resultant active forces at origin ($\mathbf{M}^{\text{o}}$, $\mathbf{F}^{\text{o}}$) are calculated by inverse dynamics without GRF. After obtaining the ZMP position, the resultant active forces at ZMP ($\mathbf{M}^{\text{zmp}}$, $\mathbf{F}^{\text{zmp}}$) are computed using the equilibrium condition as follows:

$$\begin{aligned} \mathbf{M}^{\text{zmp}} &= \mathbf{M}^{\text{o}} + {}^{\text{o}}\mathbf{r}_{\text{zmp}} \times \mathbf{F}^{\text{o}}, \\ \mathbf{F}^{\text{zmp}} &= \mathbf{F}^{\text{o}}, \end{aligned} \tag{18}$$

where ${}^{\text{o}}\mathbf{r}_{\text{zmp}}$ is the ZMP position in the global coordinate system obtained from Eqs. (16) and (17).

Then, the value and location of GRF are calculated from the equilibrium between the resultant active forces and passive forces at the ZMP:

$$\begin{aligned} &\mathbf{M}^{\text{GRF}} + \mathbf{M}^{\text{zmp}} = \mathbf{0}, \\ &\mathbf{F}^{\text{GRF}} + \mathbf{F}^{\text{zmp}} = \mathbf{0}, \\ &{}^{\text{o}}\mathbf{r}_{\text{GRF}} - {}^{\text{o}}\mathbf{r}_{\text{zmp}} = \mathbf{0}. \end{aligned} \tag{19}$$

Finally, all active forces (gravity, inertia, and external forces) and passive forces (GRF) are applied to the multibody human system to obtain the joint torques that are used in the torque limit constraints and to calculate the dynamic-effort objective function.

https://doi.org/10.1017/S0263574714000253 Published online by Cambridge University Press

*3.2. Impact in running*

Impact at foot strike has been treated in the robotics area by using the angular momentum. For example, Roussel *et al.*[29] calculated impulse by using the angular momentum as:

$$\mathbf{I} = \mathbf{J}(\mathbf{q})(\dot{\mathbf{q}}^{+} - \dot{\mathbf{q}}^{-}), \tag{20}$$

where $\mathbf{q}$ is the joint angle vector, $\dot{\mathbf{q}}^{-}$ is the joint angle velocity vector just before the foot contact, $\dot{\mathbf{q}}^{+}$ is the joint angle velocity vector just after the foot contact, $\mathbf{J}(\mathbf{q})$ is the inertia matrix, and $\mathbf{I}$ is impulse.

There is another way to calculate the impact during the foot contact that does not use velocities of the individual segments of the body. If the GRFs are known, then the concept of linear impulse can be used to formulate the impact phenomena. Newton's second law states that the force acting on a particle is equal to the rate of change of the linear momentum, i.e.,

$$\sum \mathbf{F} = m\frac{\mathrm{d}\mathbf{v}}{\mathrm{dt}}. \tag{21}$$

Integrating the equation with respect to time gives

$$\int_{t_1}^{t_2} \sum \mathbf{F}\mathrm{dt} = m\mathbf{v}_2 - m\mathbf{v}_1. \tag{22}$$

The term on the left is called linear impulse. The average with respect to time of the total force acting on an object from $t_1$ to $t_2$ is

$$\sum \mathbf{F}_{\text{average}} = \frac{1}{(t_2 - t_1)} \int_{t_1}^{t_2} \sum \mathbf{F}\mathrm{dt}. \tag{23}$$

So, with Eq. (21), we can write

$$(t_2 - t_1) \sum \mathbf{F}_{\text{average}} = m\mathbf{v}_2 - m\mathbf{v}_1. \tag{24}$$

The impulsive force is defined as a force of relatively large magnitude that acts over a small interval of time. Determining the actual history of such a force is often impractical, but its average value can be estimated.[30] Therefore, the impulse at foot strike $\mathbf{I}_{\text{strk}}$ can be approximated as

$$\mathbf{I}_{\text{strk}} = \Delta t \sum \mathbf{F}_{\text{average}}. \tag{25}$$

The GRF is the resultant external force in the current mechanical model. Therefore, impulse in terms of GRF (resultant external force) is

$$\mathbf{I}_{\text{strk}} = \mathbf{F}^{\text{GRF}} \Delta t. \tag{26}$$

The time interval is determined by numerical experimentation in this study, and the value is given in Section 7.1.

## 4. Running Model

Running is basically separated from walking in terms of whether or not both feet are off the ground during a gait cycle. The running model for the formulation is composed of two phases—the support phase and the flight phase (Fig. 3).

The support phase is further divided into three segments—foot strike, mid-support, and toe off. The terms *mid-support* and *toe off* have been adopted from the literature.[31] Figure 4 depicts these three segments of the support phase in detail.

Figure 5 depicts the foot support region in the support phase. The support region will be used in the dynamic stability constraint (ZMP constraint) and ground penetration constraint in later sections. The

https://doi.org/10.1017/S0263574714000253 Published online by Cambridge University Press

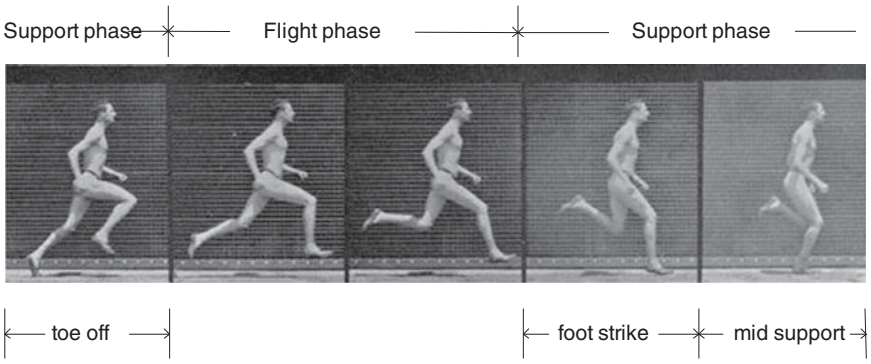



Fig. 3. Human running snapshots.

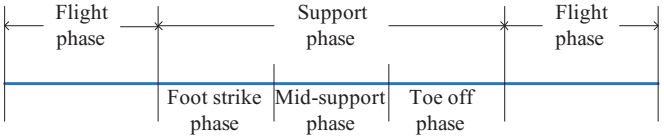



Fig. 4. Model of running phase.

black dashed area is the support region in the current formulation. According to the literature, 80% of runners strike rear foot first.[7] Therefore, it is formulated that the rear foot is the contact area in the foot-strike phase. The entire foot is the support region in the mid-support phase, and the forefoot is the support region in the toe-off phase. In the flight phase, there is no constraint on the foot. The only criterion is the conservation of angular momentum and it is embedded in the equations of motion.

## 5. Formulation of Running Problem

The running task is formulated as a nonlinear programming optimization problem. A general mathematical form is defined as: find the optimal joint trajectories $\mathbf{q}(t)$ and joint torques $\boldsymbol{\tau}(t)$ to minimize a human performance measure subject to physical constraints:

$$\begin{array}{ll} \text{Find :} & \mathbf{q}, \boldsymbol{\tau} \\ \text{To :} & \min f(\mathbf{q}, \boldsymbol{\tau}) \\ \text{Sub.} & \mathrm{h}_i = 0; i = 1, \ldots, p \\ & \mathrm{g}_j \leq 0; j = 1, \ldots, m, \end{array} \tag{27}$$

where $\mathrm{h}_i$ represents the equality constraints and $g_j$ represents the inequality constraints.

### *5.1. Design variables*

In the current formulation, the design variables are the joint angle profiles $\mathbf{q}$(t) parameterized using B-spline approximation. The joint torques $\boldsymbol{\tau}(\mathbf{q},\mathbf{t})$ are calculated using the governing differential equations. This is called the inverse dynamics procedure where the differential equations are not integrated. The number of control points in the current formulation is five for each joint angle. Since the number of DOFs for the mechanical system is 55, the total number of design variables is $55 \times 5 = 275$. The number of control points is tested through numerical simulation. The five control points are for one-step running motion. The way they are obtained is based on the principle of using a minimal number of points to capture the one-step running motion.

### *5.2. Performance measure*

The first performance measure, which is dynamic effort, is

$$f_\tau = \int_0^T \bar{\boldsymbol{\tau}}^T \bar{\boldsymbol{\tau}} \mathrm{dt}, \tag{28}$$

https://doi.org/10.1017/S0263574714000253 Published online by Cambridge University Press

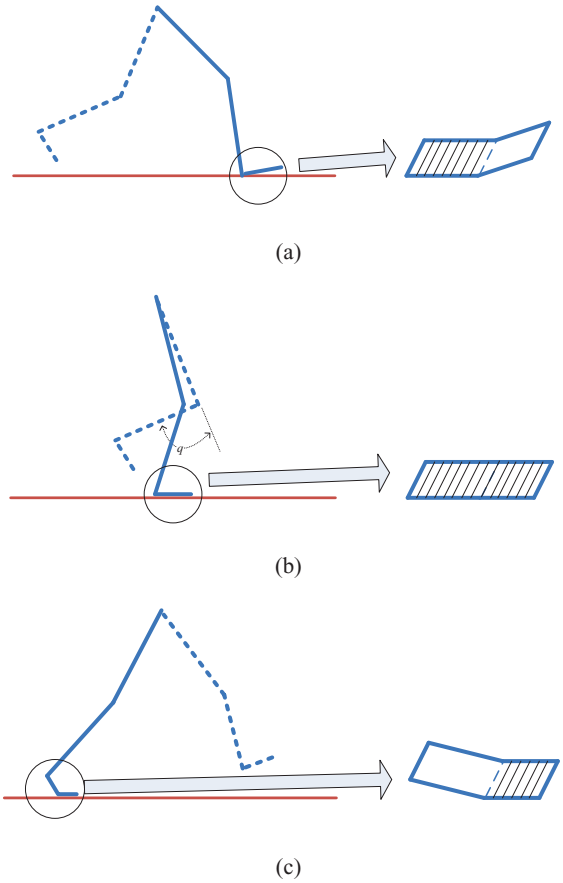



Fig. 5. Foot support phase and support region (a) foot strike; (b) mid-support; (c) toe off.

where $\bar{\boldsymbol{\tau}}$ contains the weighted joint torques as

$$\bar{\tau}_i = w_i \tau_i, \tag{29}$$

where $w_i$ is the weight coefficients. This dynamic effort is a reasonable criterion to minimize as discussed previously.[29] The impulse can be calculated from Eq. (26) once the GRFs have been calculated. Then, we can incorporate the impulse into the performance measure to minimize it. Therefore, the second performance measure is

$$f_I = \mathbf{I}_{\text{strk}}^{\text{T}} \mathbf{I}_{\text{strk}}. \tag{30}$$

Next, upper-body motion is considered for the running problem. Upper-body motion is formulated to cancel the GRF yawing moment at ZMP as

$$f_Y = \int_0^T \left(M_y^{\text{GRF}}\right)^2 \text{dt}. \tag{31}$$

Thus, the final performance measure for running formulation is

$$f = w_\tau f_\tau + w_I f_I + w_Y f_Y, \tag{32}$$

where $w_\tau$, $w_I$, and $w_Y$ are the weight values.

https://doi.org/10.1017/S0263574714000253 Published online by Cambridge University Press

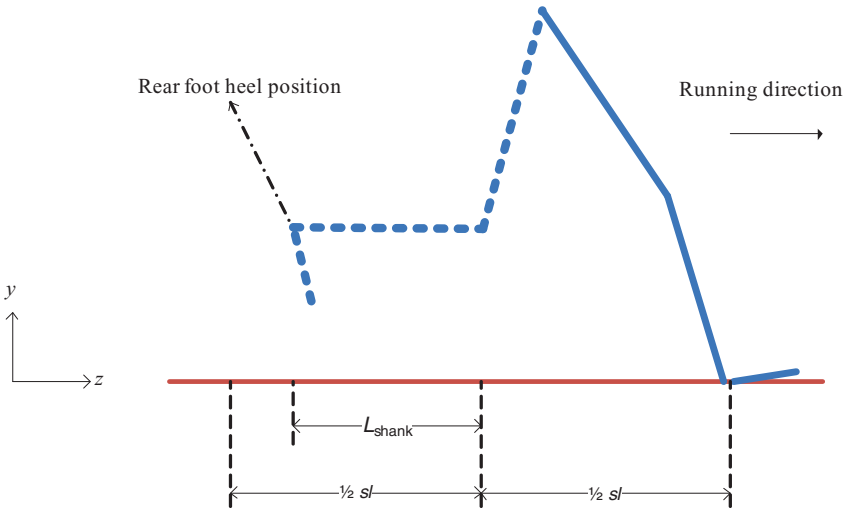



Fig. 6. Description of initial rear heel position.

### *5.3. Constraints*

*5.3.1. Joint angle limits.* Joint angle limits for the body are determined based on work by Norkin and White:[32]

$$\mathbf{q}_{\text{lower}} \leq \mathbf{q}(t) \leq \mathbf{q}_{\text{upper}} \qquad (0 \leq t \leq T). \tag{33}$$

*5.3.2. Joint torque limits.* Each joint torque is also bounded by its physical limits, which are obtained from the literature:[27,33]

$$\boldsymbol{\tau}_{\text{lower}} \leq \boldsymbol{\tau}(t) \leq \boldsymbol{\tau}_{\text{upper}} \qquad (0 \leq t \leq T), \tag{34}$$

where $\boldsymbol{\tau}_{\text{lower}}$ are the lower torque limits and $\boldsymbol{\tau}_{\text{upper}}$ the upper limits.

*5.3.3. Foot location of ground contact point.* Since the step length can be calculated from the running speed based on the literature,[27,37] the location of the foot contact points can be specified.

$$\mathbf{r}_i(t) = \tilde{\mathbf{r}}_i, \qquad (i \in \textbf{contact}), \tag{35}$$

where $\tilde{\mathbf{r}}_i$ is the specified foot location.

*5.3.4. Ground penetration.* While the foot is contacting the ground, the height of the foot from the ground is zero. While the foot is not contacting the ground, the foot should be above the ground. Then, the height of the foot from the ground is greater than zero.

$$\begin{aligned} &y_i(t) = 0, \ (i \in \textbf{contact}), \\ &y_i(t) \geq \varepsilon, \ (i \notin \textbf{contact}), \\ &\varepsilon = 10^{-3}, \end{aligned} \tag{36}$$

where $i$ refers to the contact point in the set of contact points.

*5.3.5. Initial rear heel position.* There is no boundary condition at the beginning and ending postures except the symmetry condition. Therefore, we need some constraints for creating natural motion and avoiding redundancy at $t = 0$. The rear foot heel position is controlled at the foot-strike phase to ensure that the motion looks like the middle of running. Only the $z$-directional (running direction) position is constrained by an inequality constraint at only the foot-strike phase:

$$z_{\text{RFH}} \leq \frac{1}{2} sl - L_{\text{shank}}, \tag{37}$$

https://doi.org/10.1017/S0263574714000253 Published online by Cambridge University Press

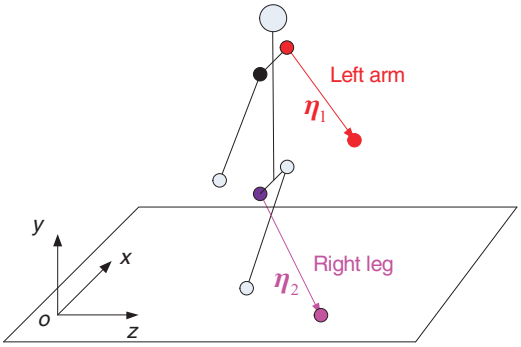



Fig. 7. Arm-leg coupling motion.

where $z_{\mathrm{RFH}}$ is the point of the rear foot heel ($z$-direction in the inertial reference frame), $sl$ is step length, and $L_{\mathrm{shank}}$ is the length of the shank. Figure 6 depicts the position $z_{\mathrm{RFH}}$ at the foot strike of the opposite foot.

*5.3.6. No-slip constraint.* The velocity of the contacting points at the foot landing instant is set to be zero (soft impact). Therefore, the following constraints are imposed:

$$\dot{\mathbf{r}}_i(t) = \mathbf{0} \qquad (i \in \textbf{contact}). \tag{38}$$

*5.3.7. ZMP constraint.* Here, the ZMP is simply a point where the moments about the $x$- and $z$-axes, due to inertia, gravity, and external force (IGF), are zero. Then, the ZMP constraint is

$$z_{\mathrm{zmp}} \in \mathrm{FSR}, x_{\mathrm{zmp}} \in \mathrm{FSR}, \tag{39}$$

where FSR is the foot support region.[16] The foot support region is described in Fig. 5.

*5.3.8. Arm-leg coupling.* It is considered that the arm swing motion helps running motion in terms of efficiency and comfort. In general, the left arm moves forward while the right leg moves forward, and the left arm moves backward while the right leg moves backward. Therefore, we constrain these arm–leg coupling directions in the sagittal plane ($z$–$y$ plane) for upper-body motion. Figure 7 depicts the arm–leg coupling motion. $\boldsymbol{\eta}_1$ is the vector from the left shoulder joint to the left elbow joint, $\eta_2$ is the vector from the right hip joint to the right knee joint, and $\mathbf{n}_z$ is the unit vector along the $z$-direction.

Then, the arm–leg coupling constraint is

$$(\boldsymbol{\eta}_1 \cdot \mathbf{n}_z)(\boldsymbol{\eta}_2 \cdot \mathbf{n}_z) \geq 0. \tag{40}$$

Note that the arm–leg coupling constraint has no relationship to obtaining the swing angles of the arm motion. It constrains only the swing direction of the arm, and the optimization process determines the swing angles.

*5.3.9. Symmetry conditions.* The running simulation starts from the left heel strike and ends with the right heel strike. The initial and final postures and velocities should satisfy the symmetry conditions to generate continuous running motion. These conditions are expressed as follows:

$$\begin{array}{ll} q_L(0) - q_R(T) = 0 & \dot{q}_L(0) - \dot{q}_R(T) = 0 \\ q_{S\mathrm{x}}(0) - q_{S\mathrm{x}}(T) = 0 & \dot{q}_{S\mathrm{x}}(0) - \dot{q}_{S\mathrm{x}}(T) = 0 \\ q_{S\mathrm{y}}(0) + q_{S\mathrm{y}}(T) = 0 & \dot{q}_{S\mathrm{y}}(0) + \dot{q}_{S\mathrm{y}}(T) = 0 \\ q_{S\mathrm{z}}(0) + q_{S\mathrm{z}}(T) = 0 & \dot{q}_{S\mathrm{z}}(0) + \dot{q}_{S\mathrm{z}}(T) = 0 \end{array}, \tag{41}$$

where subscripts $L$ and $R$ represent the DOFs of the leg, arm, and shoulder joints, which satisfy the symmetry conditions with the contra-lateral leg, arm, and shoulder joints; the subscript $S$ represents the DOFs of the spine, neck, and global joints, which satisfy the symmetry conditions on itself at the initial and final times; and $x$, $y$, $z$ are the global axes.

https://doi.org/10.1017/S0263574714000253 Published online by Cambridge University Press

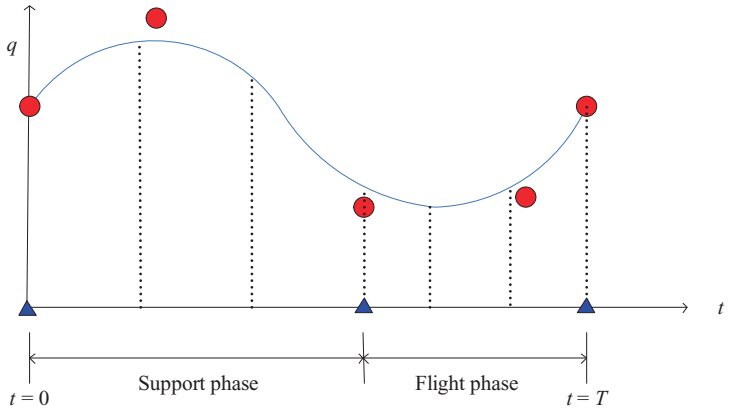



Fig. 8. Joint angle profiles parameterized in the B-spline.

## 6. Numerical Discretization and Gradients Evaluation

For the optimization problem, the time domain is discretized by using cubic B-spline curves, which are defined by a set of control points **P** and time grid points (knots) **t**. A joint profile $q(t)$ is parameterized by using B-splines as follows:

$$q(\mathbf{t}, \mathbf{P}) = \sum_{i=1}^{m} B_i(\mathbf{t}) p_i \qquad 0 \le t \le T, \tag{42}$$

where $B_i(\mathbf{t})$ are the basis functions, $\mathbf{t} = \{t_0, ..., t_s\}$ is the knot vector, and $\mathbf{P} = \{p_1, ..., p_m\}$ is the control points vector. With this representation, the control points become the optimization variables (also called the design variables). The time is distributed uniformly in the support phase between the foot-strike, mid-support, and toe-off phases.

In this study, multiplicity is used in the knot vector at the end points of the time interval. This property guarantees that the starting and ending joint angle values of a DOF are exactly those corresponding to the first and the last control point values (Fig. 8). This makes it easier to impose the symmetric posture constraints. The time-dependent constraints are imposed not only at the knot points but also between the knots, so that a very smooth motion is generated.

$$\frac{\partial C}{\partial x_k} = \frac{\partial C}{\partial q_j}\frac{\partial q_j}{\partial x_k} + \frac{\partial C}{\partial \dot{q}_j}\frac{\partial \dot{q}_j}{\partial x_k} + \frac{\partial C}{\partial \ddot{q}_j}\frac{\partial \ddot{q}_j}{\partial x_k}. \tag{43}$$

The terms $\partial q_j/\partial x_k$, $\partial \dot{q}_j/\partial x_k$, and $\partial \ddot{q}_j/\partial x_k$ can be obtained from B-spline interpolation, and the terms $\partial C/\partial q_j$, $\partial C/\partial \dot{q}_j$, and $\partial C/\partial \ddot{q}_j$ are evaluated for each constraint discussed in the previous section. In a similar way, the analytical gradient for the performance measure can be obtained. The gradient of the torque for dynamics effort is

$$\frac{\partial \tau}{\partial x_k} = \frac{\partial \tau}{\partial q_j}\frac{\partial q_j}{\partial x_k} + \frac{\partial \tau}{\partial \dot{q}_j}\frac{\partial \dot{q}_j}{\partial x_k} + \frac{\partial \tau}{\partial \ddot{q}_j}\frac{\partial \ddot{q}_j}{\partial x_k}. \tag{44}$$

From Eq. (26), the gradient of the impulse is

$$\frac{\partial \mathbf{I}_{\text{strk}}}{\partial x_k} = \left( \frac{\partial \mathbf{F}^{\text{GRF}}}{\partial q_j}\frac{\partial q_j}{\partial x_k} + \frac{\partial \mathbf{F}^{\text{GRF}}}{\partial \dot{q}_j}\frac{\partial \dot{q}_j}{\partial x_k} + \frac{\partial \mathbf{F}^{\text{GRF}}}{\partial \ddot{q}_j}\frac{\partial \ddot{q}_j}{\partial x_k} \right) \Delta t. \tag{45}$$

The terms $\partial \tau / \partial q_j$, $\partial \tau / \partial \dot{q}_j$, and $\partial \tau / \partial \ddot{q}_j$ are already evaluated in Eqs. (13)–(15).

https://doi.org/10.1017/S0263574714000253 Published online by Cambridge University Press

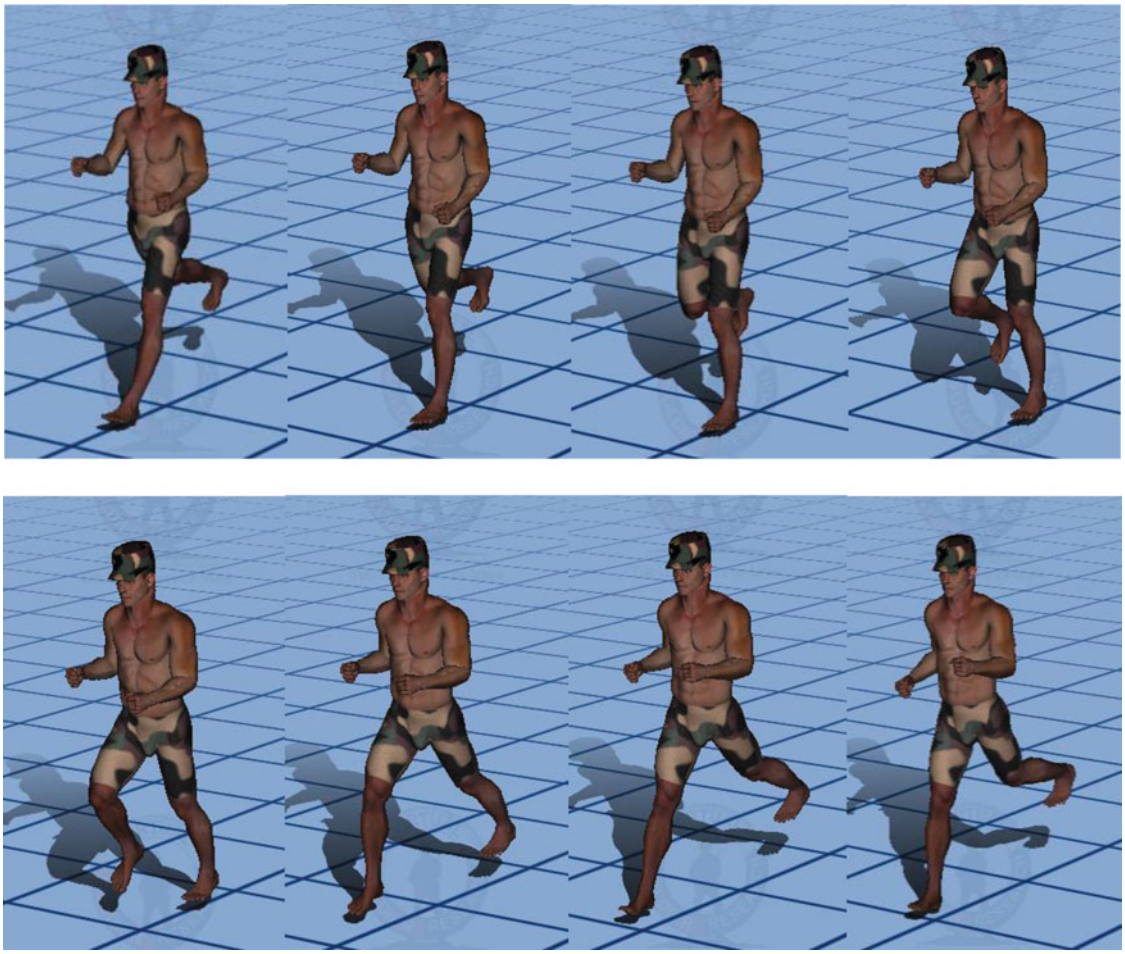


Fig. 9. Snapshot with upper-body motion formulation.

## 7. Running Simulation Results

A sequential quadratic programming (SQP) algorithm is adopted to solve the problem, and the commercial software SNOPT is used.[34] The running speed is an input parameter, and the step length is determined using the formula described in the literature. A feasible solution without a human performance measure is obtained first. Once we get a feasible solution, it is used as the starting point for optimization with the performance measure from Eq. (32).

### *7.1. Normal running*

The total number of constraints is 1060. Figure 9 shows snapshots of the simulation for 3.0 m/s running with upper-body motion formulation. Step length is 1.096 m. An Intel Core Duo 3.16 GHz CPU is used to obtain the optimal solution. The number of iterations for obtaining the feasible point is 21, and the CPU time is 417 s. The number of iterations for the optimal point is 500, and the CPU time is 297 s.

The weight values in the performance measure are set to 1.0 for the torque square term, 0.5 for the impulse term, and $1.0 \times 10^5$ for the yawing moment term. $\Delta t$ in Eq. (26) is set to 10% of support time. These values are determined by numerical experimentation. The active constraints are joint angle limits (spine, elbow, and toe), joint torque limits (ankle), ground penetration, no slip, ZMP, foot location, arm-leg coupling, and symmetry condition constraints.

Figures 10 and 11 show the knee joint torque profile, the vertical GRF results, and their comparisons with the results without upper-body motion formulation. The trends of the results are similar.

https://doi.org/10.1017/S0263574714000253 Published online by Cambridge University Press

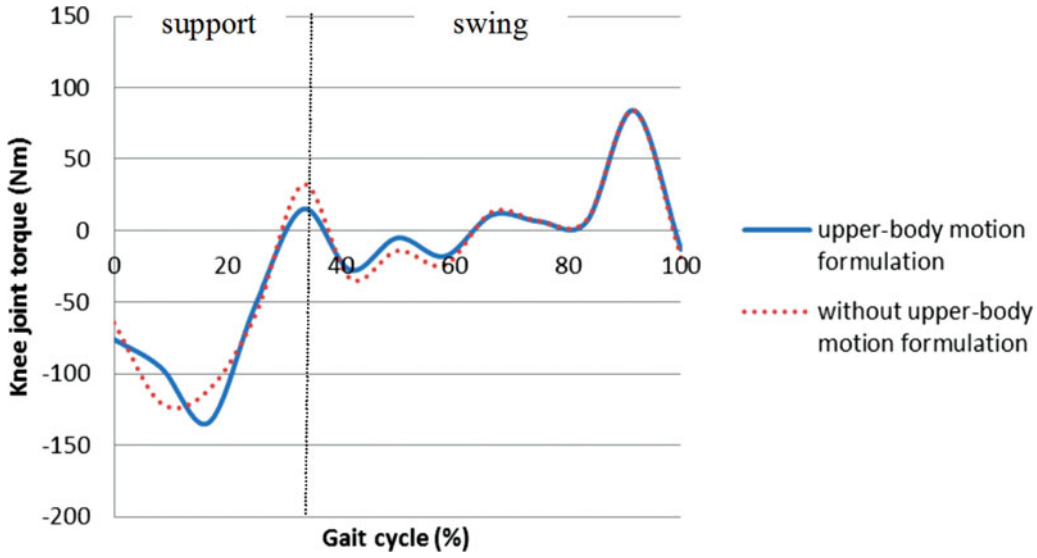



Fig. 10. Knee joint torque profiles.

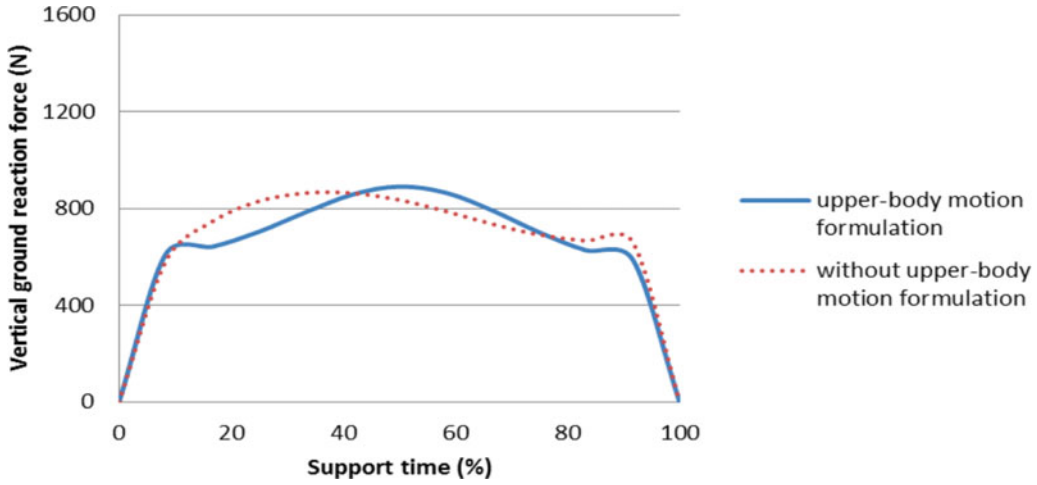



Fig. 11. Vertical ground reaction force.

### *7.2. Validation of normal running*

Six determinants (hip flexion/extension, knee flexion/extension, ankle flexion/extension, pelvic tilt, pelvic rotation, and lateral pelvic displacement) were chosen to validate the running simulation. Experiments were performed by our validation group, and data were obtained for five healthy male subjects.[35,36] Each subject ran at normal running speeds. These results are normalized for the running cycle. The running speed of the simulation is 3.0 m/s. Figure 12 shows the validation results. The average values are used for the swing and support phases. Also, Fig. 12 shows the average of the five subjects.

In Fig. 12, the blue dotted curves are the 95% confident region of the statistical means, the thick black curves are the mean value of the experimental data, and the thin red curves are the simulation results. Pelvic displacement is the displacement of lateral pelvic movement. In general, the trend of red curves (simulation) follows the experimental results.

### *7.3. Different running speeds*

Figure 13 shows the knee joint torques with different running speeds, 3.0 m/s, 3.5 m/s, and 4.0 m/s, respectively. From the figure, we can observe that the peak value of joint torque gets larger when the running speed increases. In addition, the human inclines his torso and swings his arm at large amplitude when the running speed increases.

https://doi.org/10.1017/S0263574714000253 Published online by Cambridge University Press

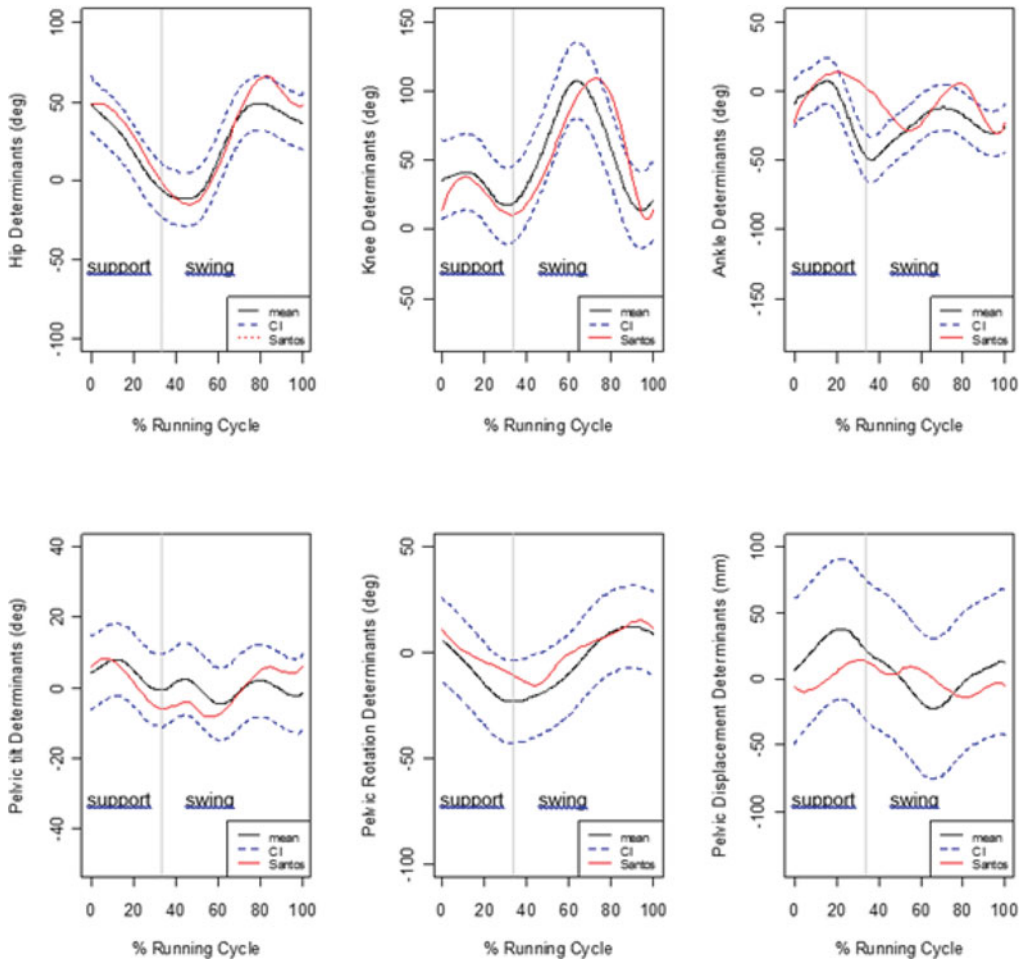



Fig. 12. Running validation – six determinants.

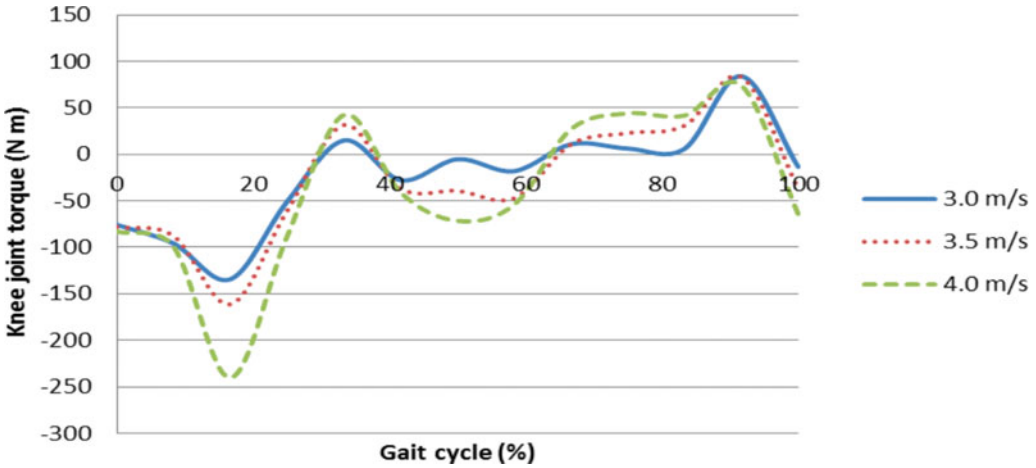



Fig. 13. Knee joint torque at different running speeds.

Figure 14 shows the vertical GRF for different running speeds. Also, it is observed that the peak value of the GRF gets larger when the running speed increases.

The common active constraints for all cases are ground penetration, no slip, foot contact, ZMP, arm-leg coupling, and symmetry conditions. Table I shows the summary of results in the cause and effect case study with different running speeds.

https://doi.org/10.1017/S0263574714000253 Published online by Cambridge University Press

Table I. Summary of results—running speed case study.

| Case | | 3.0 m/s | 3.5 m/s | 4.0 m/s |
|---|---|---|---|---|
| Number of iteration | | 500 | 324 | 354 |
| Performance measure | | 11,079 | 13,665 | 20,713 |
| Active constraints | | 146 | 191 | 189 |
| Peak knee torque (Nm) | | –134.30 | –161.39 | –240.30 |
| Peak GRF (N) | Vertical | 891.06 | 967.12 | 1007.02 |
| | Forward (FS/TO) | –289.89/372.23 | –470.87/369.99 | –361.41/383.39 |
| | Lateral | 74.14 | 162.03 | 243.43 |

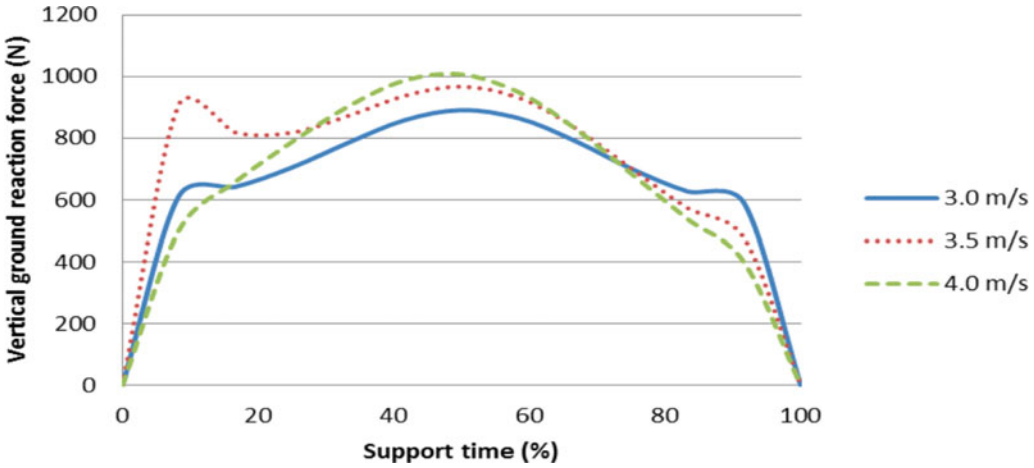



Fig. 14. Vertical ground reaction force at different running speeds.

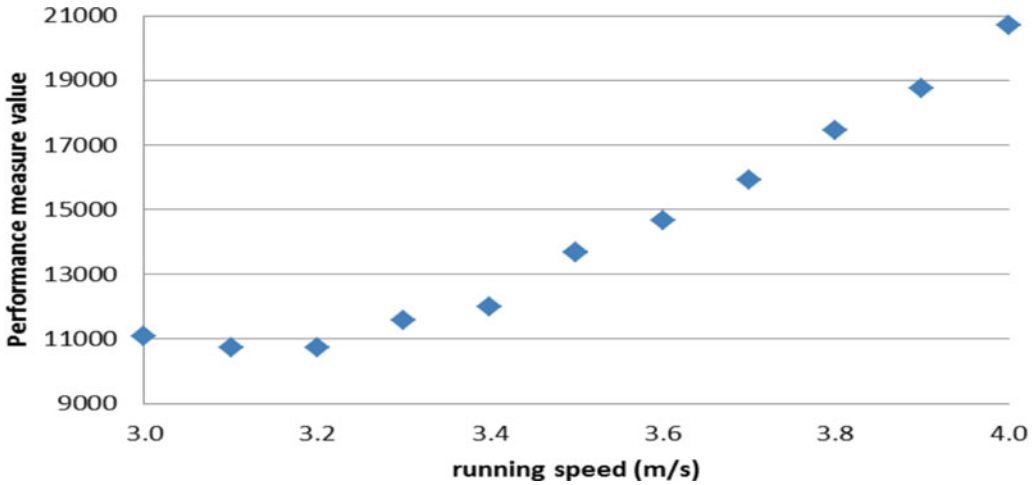



Fig. 15. Performance measure values for different running speeds.

Figure 15 shows the performance measure values for different running speeds. We can observe that the performance measure value gradually increases when the running speed increases.

### *7.4. Effects of foot location*

In this section, we study the effect of foot location from the center line of running and determine if the foot location has an effect on natural running motion. Then, we can use the good results from this study in later studies.

Figure 16 depicts the different foot location cases for the running formulation. $D_f$ in Fig. 16(a) is the distance between the center lines of the foot and running direction. Figure 16(b) shows the case in

https://doi.org/10.1017/S0263574714000253 Published online by Cambridge University Press

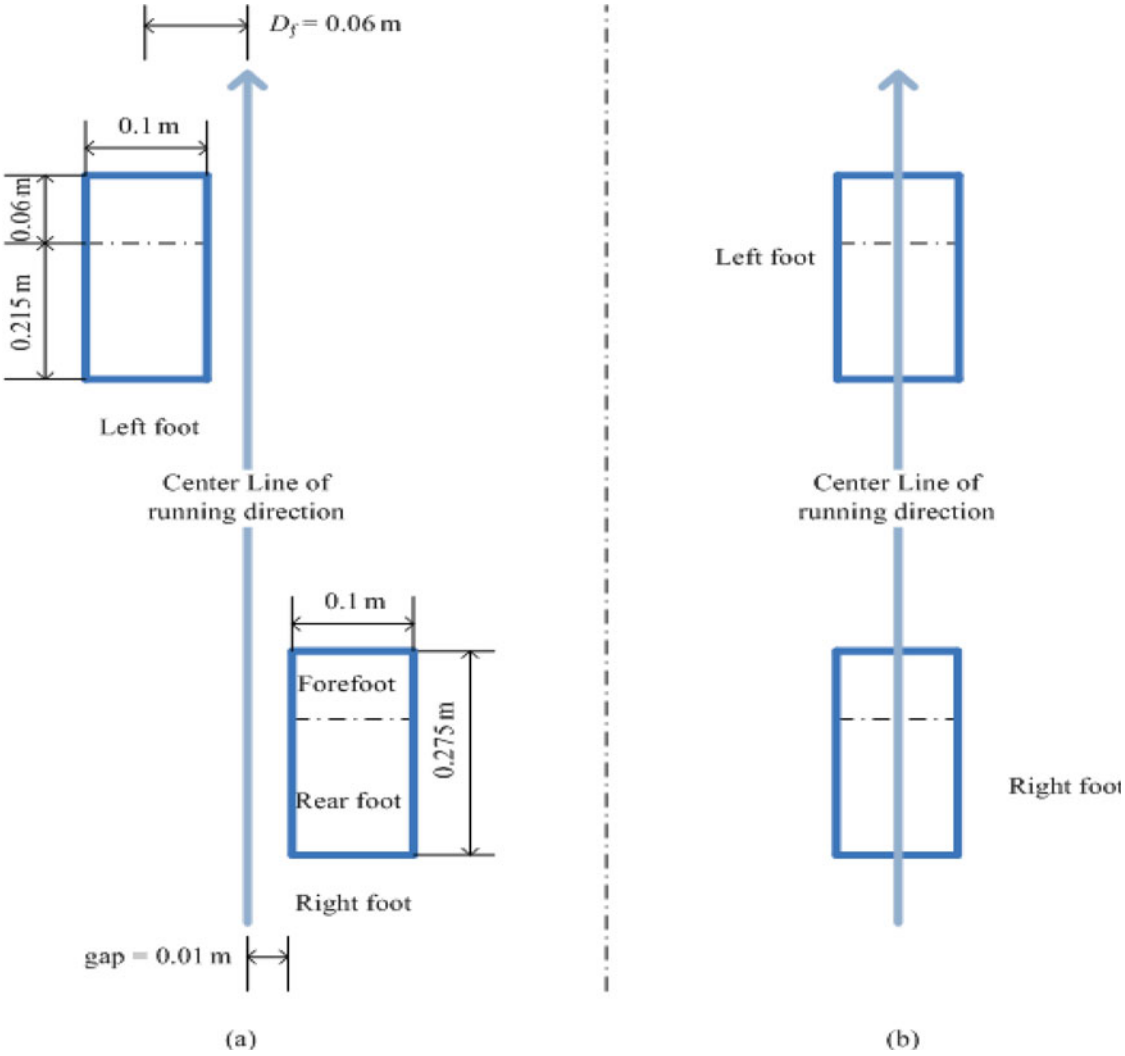



Fig. 16. Foot locations in running.

which the foot is located on the center line of the running direction ($D_f = 0.0$ m). Figures 17 and 18 are snapshots of running at 3.7 m/s with $D_f$ as 0.06 m and 0.0 m, respectively. Figure 19 is snapshot of the results where $D_f$ is 0.085 m.

As an extreme case, $D_f$ of 0.35 m is specified. The optimization algorithm reports an infeasible problem with this constraint. The violated constraints are ZMP, foot location, and joint torque limits. For joint torque limit constraints, the spine joint and the right and left hip joints are violated. However, when the joint torque limits are relaxed to double their normal values for all joints, an optimal solution is found. Then, the active constraints are joint angle limits (right and left ankles), ground penetration, no-slip, ZMP, foot location, arm–leg coupling, and the symmetry condition constraints. Figure 20 is snapshot of the results. We can observe that the upper body is leaning toward the next step for stability in this case.

We can observe that the motion in Fig. 17 is quite natural. Also, we can note that the hip is rotating too much when $D_f$ is 0.0 m in Fig. 18 and that the leg swings outward where $D_f$ is 0.085 m in Fig. 19. Therefore, we can use $D_f$ as 0.06 m for later studies. Table II contains a summary of the results of this cause and effect case study – the foot locations.

### *7.5. Effects of foot orientation*

The formulation of running in Section 6 is for a straight path; there is an assumption that the motion is symmetric. However, a slow jog along a curve is not a symmetric motion since the motions for

https://doi.org/10.1017/S0263574714000253 Published online by Cambridge University Press

Table II. Summary of results—foot locations case study (running speed = 3.7 m/s).

| Case | | $D_f = 0.06$ m | $D_f = 0.0$ m | $D_f = 0.085$ m | $D_f = 0.35$ m |
|---|---|---|---|---|---|
| Number of iteration | | 24 | 201 | 359 | 85 |
| Performance measure | | 15,921 | 19,466 | 15,624 | 45,662 |
| Active constraints | | 191 | 189 | 207 | 144 |
| Peak knee torque (Nm) | | –200.10 | –189.45 | –192.70 | –253.62 |
| Peak GRF (N) | Vertical | 944.41 | 974.18 | 880.11 | 1163.61 |
| | Forward (FS/TO) | –475.24/349.73 | –382.55/352.98 | –422.25/304.18 | –100.52/887.73 |
| | Lateral | 208.77 | 208.91 | 174.32 | –759.90 |

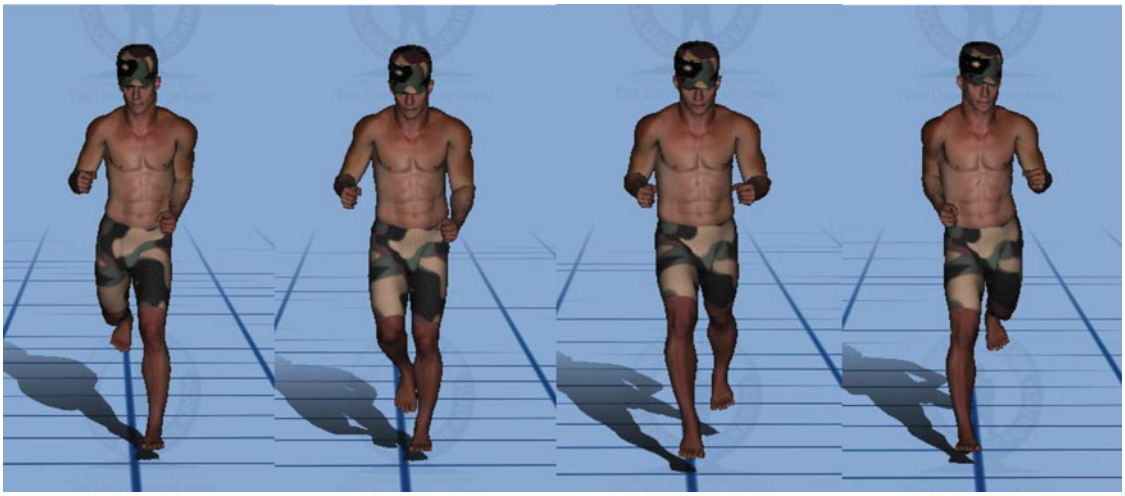


Fig. 17. Snapshot of running at $D_f = 0.06$ m.

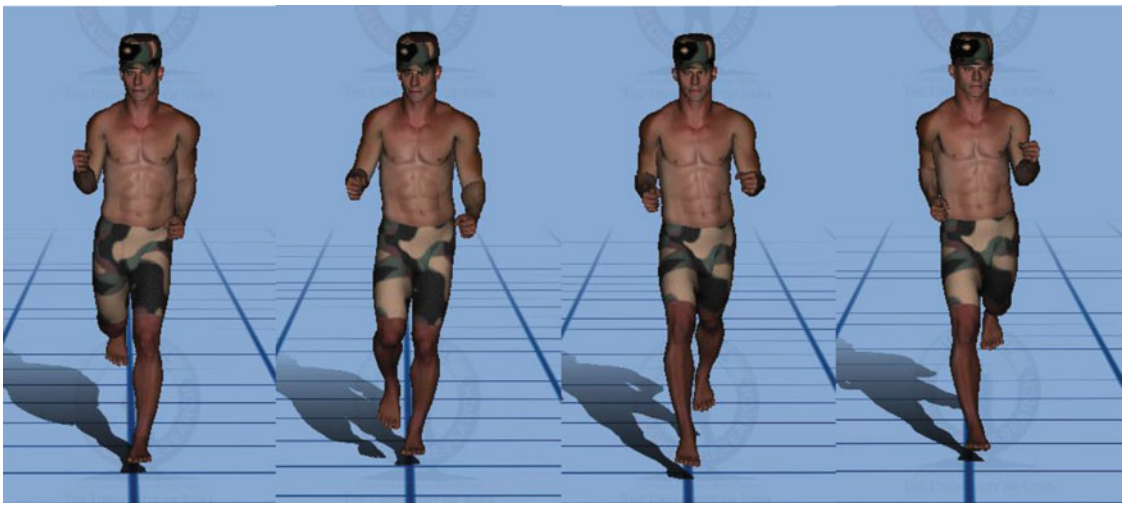


Fig. 18. Snapshot of running at $D_f = 0.0$ m.

the right and left parts of the body are not the same. Figure 21 depicts the running path of a slow jog along a circular path. The blue dot is a marker and the red curve is the circular path around the marker. Since it is a non-symmetric running motion, the right step and left step should be formulated and simulated separately (stride formulation).

Figure 22 depicts the continuity constraint. This constraint is imposed at the beginning of each optimization so that the last posture of the previous optimization and the starting posture of the current

https://doi.org/10.1017/S0263574714000253 Published online by Cambridge University Press

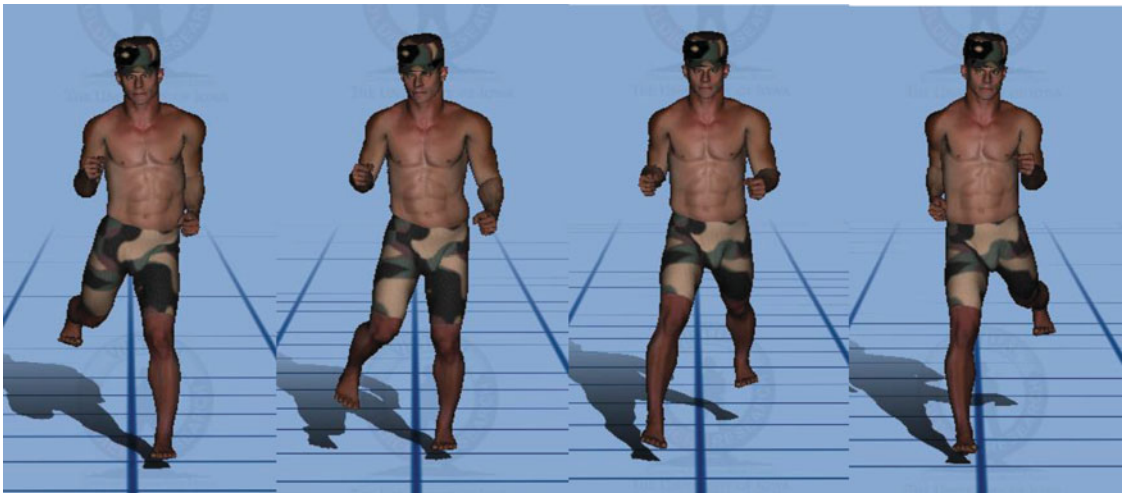


Fig. 19. Snapshot of running at $D_f = 0.085$ m.

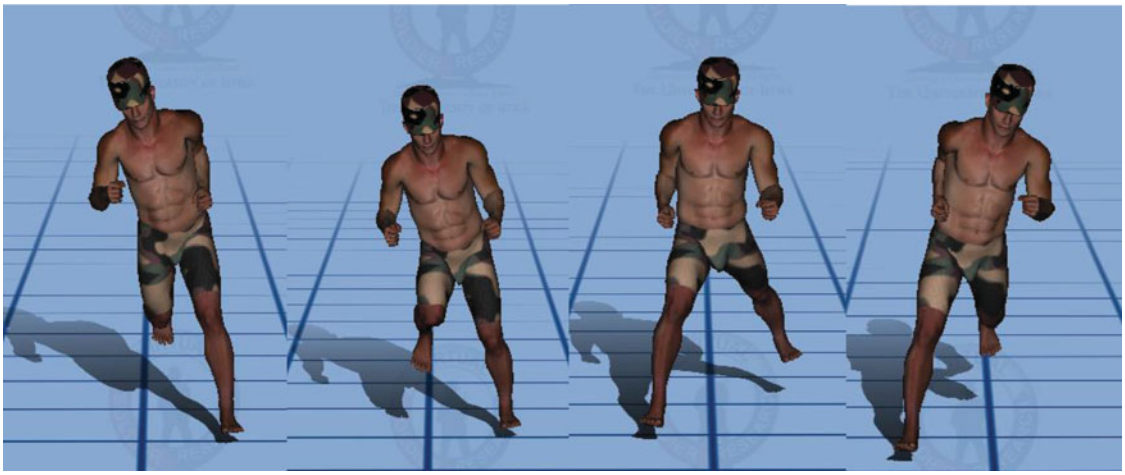


Fig. 20. Snapshot of running at $D_f = 0.35$ m.

optimization are matched. Thus, the continuity constraint is

$$\mathbf{x}_{1\text{st}}(T) = \mathbf{x}_{2\text{nd}}(0), \tag{46}$$

where $\mathbf{x}_{1\text{st}}$ represents the control points of the first optimization problem and $\mathbf{x}_{2\text{nd}}$ represents the control points of the second optimization problem.

For the problem of a slow jog along curves, the foot contact locations depend on the running path. To impose a foot contact location constraint, we constrain three points on the foot—heel, mid-foot, and toe—just as for the normal running formulation. To calculate the contacting location of these points, we need the step length and orientation of the foot. This orientation must be expressed in the inertial reference frame. Once we have the step length and the orientation of the foot, we can calculate the location of the three contact points—heel, mid-foot, and toe.

Figure 23 depicts the foot location along the path. The blue box describes the foot on the ground. $x$–$z$ is the inertial reference frame and $x_1$–$z_1$ is the local reference frame for the foot. $\mathbf{r}_p$ is the vector from the origin of the inertial reference frame to the foot point p, which will be controlled in the local reference frame. $\mathbf{r}_1$ is the vector from the origin of the inertial reference frame to the origin of the local reference frame. $\mathbf{r}_{1p}$ is the vector from the origin of the local reference frame to the foot point p in the local reference frame. What we need is $\mathbf{r}_p$ since the foot location constraint is applied in the inertial reference frame.

https://doi.org/10.1017/S0263574714000253 Published online by Cambridge University Press

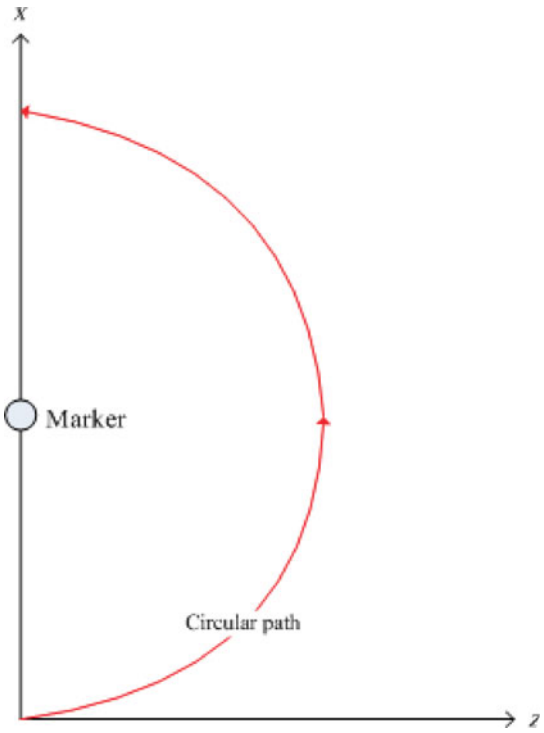



Fig. 21. Circular path around marker.

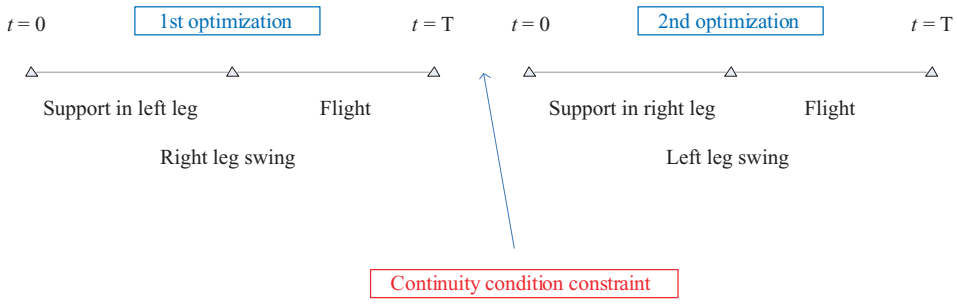



Fig. 22. Continuity condition constraint.

The vector $\mathbf{r}_1$ is determined by the step length and running curve:

$$\|\mathbf{r}_1\| = L, \tag{47}$$

where $L$ is step length. The angle $\theta$, which is the same as the orientation of the contacting foot, can be calculated from the marker position.

$$\theta = 2\sin^{-1}\left(\frac{L}{2R}\right). \tag{48}$$

Then the vector of point p can be written as

$$\mathbf{r}_p = \mathbf{r}_1 + \mathbf{A}_1\mathbf{r}_{1p}, \tag{49}$$

where $\mathbf{A}_1$ is the rotation matrix of the local reference frame.

https://doi.org/10.1017/S0263574714000253 Published online by Cambridge University Press

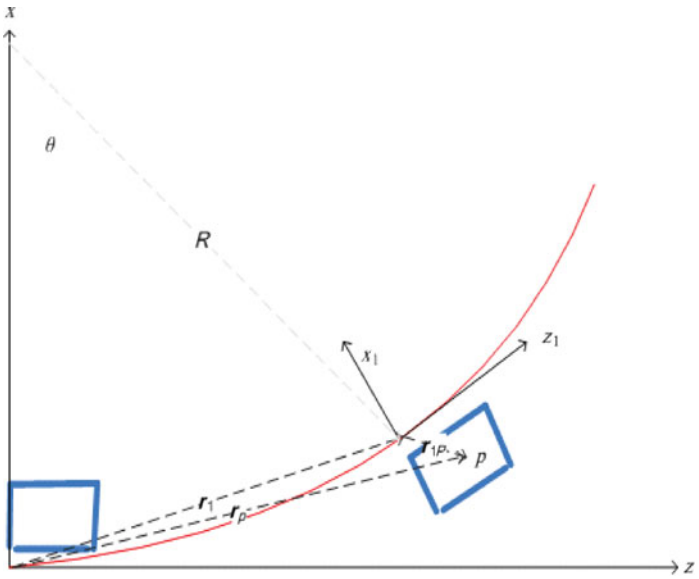



Fig. 23. Foot location along the path.

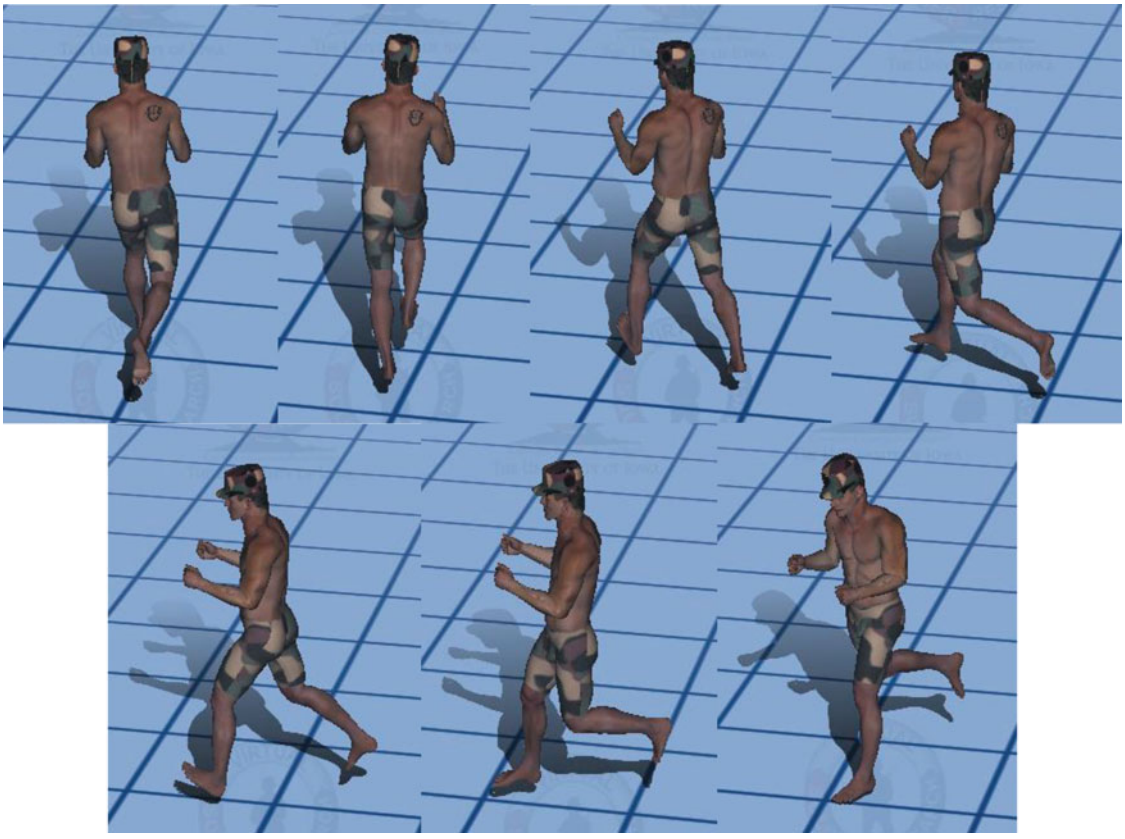


Fig. 24. Slow jog along curve snapshot.

Or,

$$\mathbf{r}_p = \begin{bmatrix} 2R\sin(\theta/2)\cos(\theta/2) + z_{1p}\cos\theta - x_{1p}\sin\theta \\ 2R\sin(\theta/2)\sin(\theta/2) + z_{1p}\sin\theta + x_{1p}\cos\theta \end{bmatrix}. \tag{50}$$

The point p is defined as heel, mid-point, and toe in the current formulation.

https://doi.org/10.1017/S0263574714000253 Published online by Cambridge University Press

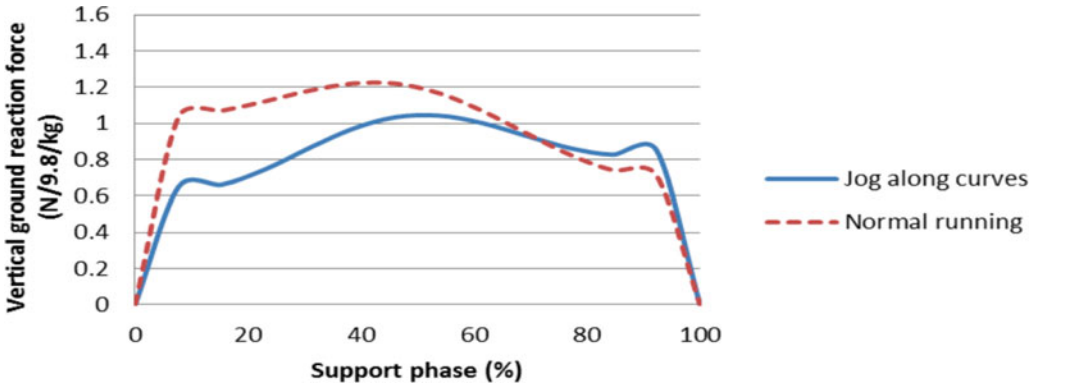



Fig. 25. Vertical ground reaction force.

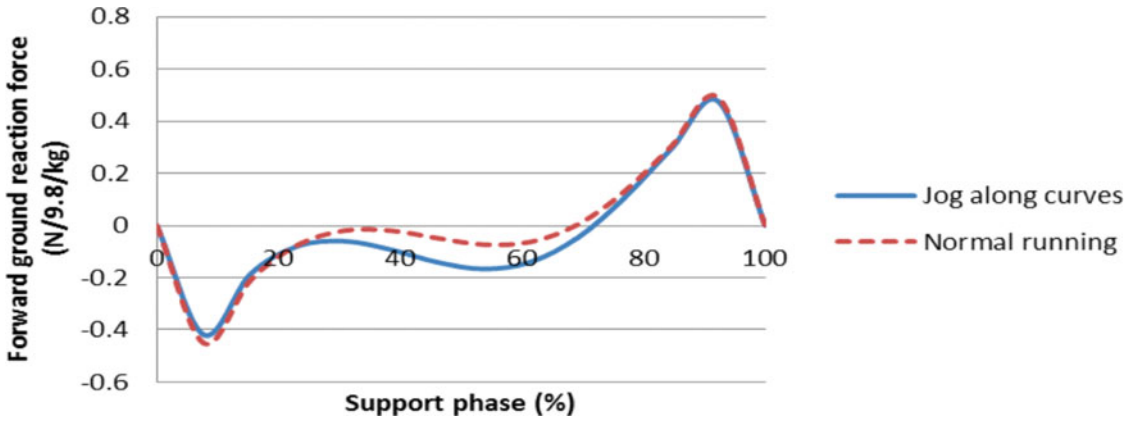



Fig. 26. Forward ground reaction force.

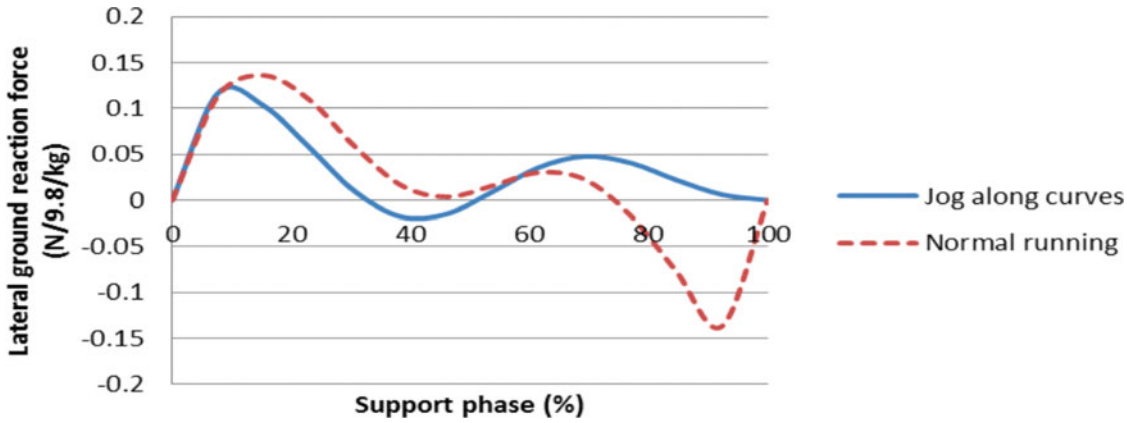



Fig. 27. Lateral ground reaction force.

The problem has been solved using the stride formulation. Therefore, there are two optimization processes—right step and left step. Once the solution has been obtained, the motion is repeated along the running path. Figure 24 is a snapshot of postures for a 2.35 m/s slow jog around a marker. Step length is 0.889 m. The number of constraints is 994. The feasible point from normal running in Section 7.1 was used as the starting point for optimization. The number of iterations for the optimal point is 16, and the CPU time is 244 s for the first step—the right step. For the second step—the left step—the number of iterations is 25 and the CPU time is 923 s. The performance measure value is 3736 for the first step and 3023 for the second step.

Figures 25–27 show the results of the GRFs.

https://doi.org/10.1017/S0263574714000253 Published online by Cambridge University Press

Results show that the trends of the vertical and forward GRFs of a slow jog along a curve are similar to the normal running case. However, the lateral GRF is quite different. Most of the GRF for a jog along a curve is in a positive area. This shows that the lateral GRF is produced to turn the body in the direction of the motion.

## 8. Concluding Remarks

In this paper, a formulation to predict the running motion of a 55-DOF digital human model was presented. The normal running was treated as a cyclic and symmetric motion with repeatable initial and final postures. The motion planning was formulated as a large-scale nonlinear programming problem that was solved using the SQP algorithm. Joint profiles were discretized using cubic B-splines and the corresponding control points were treated as unknowns. The energy-related objective function, integral of squares of all joint torques, was minimized with impulse. Due to its crucial role in running, the arm motion was incorporated by considering the arm–leg motion coupling constraint and yawing moment cancellation in the formulation. Data for the six standard running determinants were obtained from experiments with human subjects and were used to verify the simulated running motion. The effect of running speed was studied and reasonable simulations were obtained. The current formulation was shown to be very effective in obtaining joint torques and GRFs. Finally, the proposed skeletal model, problem formulation, and solution procedure predicted both kinematics and dynamics of human running quite accurately. Furthermore, the problem of a slow jog along curved paths has been formulated. It is a non-symmetric running motion, so the stride formulation has been used. A jogging path is defined as a circular curve around the marker with a given radius. For future research, more extensive validation of the approach using more subjects will be performed.

## Acknowledgements

This research was supported by projects from TACOM and the Natick Soldier Research Center.

## References

1. Y. Fujimoto, "Trajectory Generation of Biped Running Robot with Minimum Energy Consumption," *Proceedings of the IEEE international Conference on Robotics and Automation*, New Orleans, USA (Apr. 26–May 1, 2004) pp. 3803–3808.
2. J. K. Hodgins, "Three-Dimensional Human Running," *Proceedings of the International Conference on Robotics and Automation*, Minneapolis, USA (Apr. 22–28, 1996) pp. 3271–3276.
3. K. Hirai, M. Hirose, Y. Haikawa and T. Takenaka, "The Development of Honda Humanoid Robot," *Proceedings of the IEEE international Conference on Robotics and Automation*, Leuven, Belgium (May 16–20, 1998) pp. 1321–1326.
4. Y. Kim, B. Lee, J. Yoo, S. Choi and J. Kim, "Humanoid Robot HanSaRam: Yawing Moment Cancellation and ZMP Compensation," *Proceedings of AUS International Symposium on Mechatronics*, Sharjah, U.A.E (Apr. 19–21, 2005).
5. X. Mu and Q. Wu, "Synthesis of a complete sagittal gait cycle for a five-link biped robot," *Robotica* **21**, 581–587 (2003).
6. T. Nagasaki, S. Kajita, K. Yokoi, K. Kaneko and K. Tanie, "Running Pattern Generation and its Evaluation using a Realistic Humanoid Model," *Proceedings of the IEEE International Conference on Robotics and Automation*, Taipei, Taiwan (Sep. 14–19, 2003) pp. 1336–1342.
7. T. Novacheck, "Review paper: The biomechanics of running," *Gait Posture* **7**, 77–95 (1998).
8. S. Õunpuu, "The biomechanics of walking and running," *Clin. Sports Med.* **13**(4) 843–863 (1994).
9. J. Park and O. Kwon, "Impedance Control for Running of Biped Robots," *Proceedings of the IEEE/ASME International Conference on Advanced Intelligent Mechatronics* (Jul. 20–24, 2003) pp. 944–949.
10. Y. Xiang, J. S. Arora and K. Abdel-Malek, "Physics-based modeling and simulation of human walking: A review of optimization-based and other approaches," *Struct. Multidiscip. Optim.* **42**, 1–23 (2010).
11. M. J. Milliron and P. R. Cavanagh, "Sagittal Plane Kinematics of the Lower Extremity during Distance Running," **In**: *Biomechanics of Distance Running* (P. R. Cavanagh, ed.) (Human Kinetics, Champaign, IL, 1990) pp. 65–105.
12. K. Simpson and B. Bates, "The effects of running speed on lower extremity joint moments generated during the support phase," *Int. J. Sport Biomech.* **6**, 309–324 (1990).
13. J. S. Arora, *Introduction to Optimum Design*, 3rd ed. (Academic Press, San Diego, USA, 2012).
14. M. Hardt, O. von Stryk, D. Wollherr and M. Buss, "Development and Control of Autonomous, Biped Locomotion using Efficient Modeling, Simulation, and Optimization Techniques," *Proceeding of IEEE International Conference on Robotics and Automation*, Taipei, Taiwan (Sep. 14–19, 2003) pp. 1356–1361.

https://doi.org/10.1017/S0263574714000253 Published online by Cambridge University Press

15. O. von Stryk and R. Bulirsch, "Direct and indirect methods for trajectory optimization," *Ann. Oper. Res.* **37**, 357–373 (1992).
16. Y. Xiang, J. S. Arora, S. Rahmatalla and K. Abdel-Malek, "Optimization-based dynamic human walking prediction: One step formulation," *Int. J. Numer. Methods Eng.* **79**(6), 667–695 (2009).
17. Y. Xiang, J. S. Arora and K. Abdel-Malek, "Optimization-based prediction of asymmetric human gait," *J. Biomech.* **44**(4), 683–693 (2011).
18. Y. Xiang, J. S. Arora, S. Rahmatalla, T. Marler, R. Bhatt and K. Abdel-Malek, "Human lifting simulation using a multi-objective optimization approach," *Multibody Syst. Dyn.* **23**(4), 431–451 (2010).
19. Y. Xiang, J. S. Arora and K. Abdel-Malek, "3D human lifting motion prediction with different performance measures," *Int. J. Humanoid Robot.* **9**(2), 1250012 (2012).
20. Y. Xiang, H. J. Chung, J. H. Kim, R. Bhatt, S. Rahmatalla, J. Yang, T. Marler, J. S. Arora and K. Abdel-Malek, "Predictive dynamics: An optimization-based novel approach for human motion simulation," *Struct. Multidiscip. Optim.* **41**(3), 465–479 (2010).
21. Y. Xiang, J. S. Arora and K. Abdel-Malek, "Hybrid predictive dynamics: A new approach to simulate human motion," *Multibody Syst. Dyn.* **28**(3), 199–224 (2012).
22. J. H. Kim, Y. Xiang, J. Yang, J. S. Arora and K. Abdel-Malek, "Dynamic motion planning of overarm throw for a biped human multibody system," *Multibody Syst. Dyn.* **24**(1), 1–24 (2010).
23. S. Collins, P. Adamczyk and A. D. Kuo, "Dynamic Arm Swinging in Human Walking," *Proc. R. Soc. Biol. Sci.* **276**, 3679–3688 (2009).
24. J. Denavit and R. S. Hartenberg, "A kinematic notation for lower-pair mechanisms based on matrices," *ASME J. Appl. Mech.* **22**, 215–221 (1955).
25. J. M. Hollerbach, "A recursive Lagrangian formulation of manipulator dynamics and a comparative study of dynamics formulation complexity," *IEEE Trans. Syst. Man Cybern.* **11**(10), 730–736 (1980).
26. Y. Xiang, J. S. Arora and K. Abdel-Malek, "Optimization-based motion prediction of mechanical systems: Sensitivity analysis," *Struct. Multidiscip. Optim.* **37**(6), 595–608 (2009).
27. H. J. Chung, Optimization-Based Dynamic Prediction of 3D Human Running *Ph.D. Thesis* (Iowa City, IA: The University of Iowa, 2009).
28. M. Vukobratović and B. Borovac, "Zero-moment point - thirty five years of its life," *Int. J. Humanoid Robot.* **1**(1), 157–173 (2004).
29. L. Roussel, C. Canuda-de-Wit and A. Goswami, "Generation of Energy Optimal Complete Gait Cycles for Biped Robots," *Proceedings of the IEEE International Conference on Robotics and Automation*, Leuven, Belgium (May 16–20, 1998) pp. 2036–2041.
30. A. Bedford and W. Fowler, *Engineering Mechanics: Dynamics*, 3rd ed. (Prentice Hall, New Jersey, 2002).
31. K. R. Williams and P. R. Cavanagh, "Relationship between distance running mechanics, running economy, and performance," *J. Appl. Phys.* **63**(3), 1236–1245 (1987).
32. C. C. Norkin and D. J. White, *Measurement of Joint Motion: A Guide to Goniometry*, 3rd ed. (F. A. Davis Co, Philadelphia, 2003).
33. Y. Xiang, J. S. Arora, H. J. Chung, H. J. Kwon, S. Rahmatalla, R. Bhatt and K. Abdel-Malek, "Predictive simulation of human walking transitions using an optimization formulation," *Struct. Multidiscip. Optim.* **45**(5), 759–772 (2012).
34. P. E. Gill, W. Murray and M. A. Saunders, "SNOPT: An SQP algorithm for large-scale constrained optimization," *SIAM J. Optim.* **12**, 979–1006 (2002).
35. S. Rahmatalla, Y. Xiang, R. Smith, J. Meusch and R. Bhatt, "A validation framework for predictive human models," *Int. J. Hum. Factors Modelling Simul.* **2**(1/2), 67–84 (2011).
36. Y. Xiang, S. Rahmatalla, J. S. Arora and K. Abdel-Malek, "Enhanced optimisation-based inverse kinematics methodology considering joint discomfort," *Int. J. Hum. Factors Modelling Simul.* **2**(1/2), 111–126 (2011).
37. A. Bruderlin and T. Calvert, "Knowledge-Driven, Interactive Animation of Human Running," *Proceedings of the Conference on Graphics Interface*, Toronto, Canada (May 22–24, 1996) pp. 213–221.
38. J. H. Kim, Y. Xiang, R. Bhatt, J. Yang, H. J. Chung, J. S. Arora and K. Abdel-Malek, "Generating effective whole-body motions of a human-like mechanism with efficient ZMP formulation," *Int. J. Robot. Autom.* **24**(2), 125–136 (2009).

https://doi.org/10.1017/S0263574714000253 Published online by Cambridge University Press